

Signatures of valley drift in the diversified band dispersions of bright, gray, and dark excitons in MoS₂ monolayers under uni-axial strains

Ching-Hung Shih,[†] Guan-Hao Peng,[‡] Ping-Yuan Lo,[‡] Wei-Hua Li,[‡] Mei-Ling Xu,[‡] Chao-Hsin Chien,^{*,†} and Shun-Jen Cheng^{*,‡}

[†]*Institute of Electronics, National Yang Ming Chiao Tung University, Hsinchu 300, Taiwan*

[‡]*Department of Electrophysics, National Yang Ming Chiao Tung University, Hsinchu 300, Taiwan*

E-mail: chchien@nycu.edu.tw; sjcheng@nycu.edu.tw

Abstract

We present a comprehensive theoretical investigation of the strain-modulated excitonic properties of uni-axially strained transition-metal dichalcogenide monolayers (TMD-MLs) by solving the Bethe-Salpeter equation (BSE) established on the basis of first principles. We show that imposing an uni-axial strain onto a MoS₂ monolayers leads to the diversified band dispersions of the bright exciton (BX), gray exciton (GX), and dark exciton (DX) states, as a consequence of the competitive interplay between strain-induced valley drift (VD) and momentum-dependent electron-hole exchange interaction (EHEI). While the band dispersions of BX doublet in the light-accessible small reciprocal area remain almost unchanged against strain, the band dispersion of DX is reshaped by an increasing uni-axial strain from a parabola to a Mexican-hat-like profile, featured with unusual sign-reversal of the heavy effective mass and strain-activated brightness. In contrast, the effective mass of GX is drastically lightened by uni-axial strain and remains always positive. We show that the strain-diversified exciton band dispersions leads to the distinct exciton diffusivities and angle-resolved optical patterns of BX, GX, and DX in a strained TMD-ML, suggesting the feasibility of *spatially* resolving spin-allowed and -forbidden excitons in exciton transport experiments and angle-resolved optical spectroscopies.

Keywords

Dark Exciton, 2D materials, uni-axial strain, MoS₂, exciton diffusion, angle-resolved photoluminescence, valley drift

Transition metal dichalcogenide (TMD) monolayers (MLs) have been known as a promising low-dimensional material for valley-based photonic and excitonic applications.¹⁻⁷ Because of enhanced electron-hole (*e-h*) Coulomb interactions in the 2D systems, photo-excited TMD-MLs exhibit pronounced exciton fine structures,⁸⁻¹⁰ allowing for spec-

trally resolving exciton complexes in variety, including spin-allowed bright excitons (BXs) and spin-forbidden gray (GX) and dark excitons (DXs),¹¹⁻¹⁵ and serving as a platform for exciton-based optoelectronic applications.¹⁶⁻²² In particular, atomically thin TMD-MLs present high mechanical flexibility that can withstand the strain even so high as 10%²³

and suggests the prospect of TMD-based straintronics.²⁴ To date, effective mechanical control of the electronic and optical properties of TMD-MLs, comprising WSe₂, MoS₂, WSe₂ and MoSe₂ monolayers, has been demonstrated by applying bi-axial,^{25–27} uni-axial,^{28–30} and non-uniform strains as well.^{31,32} Remarkably, imposing a uni-axial strain to a crystalline material can fundamentally transform the inherent crystal symmetry and often gives rise to peculiar electronic and excitonic structures. It has been experimentally shown that imposing uni-axial strains on TMD-MLs leads to direct-indirect band gap transitions,^{28,33,34} strain-induced fine structure splitting of BX,^{35,36} strain-guided exciton transport,^{37,38} formation of quasi-1D localized exciton,³⁹ and valley drift (VD).^{40,41}

Regarding the strain-induced VD, the band edge states of conduction and valence bands of a uni-axially strained TMD-ML was predicted by the density functional theory (DFT) to be relocated apart from the K- and K'-points in the reciprocal space.^{42–44} Such a strain-induced VD has been shown to generate Berry curvature dipoles, leading to non-linear Hall conductivities⁴⁵ and valley orbital magnetization, as experimentally observed in Refs. 40,41,46. Notably, the VDs of conduction and valence bands caused by a common uni-axial strain in a TMD-ML are towards the same direction but follow different displacements in the momentum space. The unequal momentum VDs of conduction and valence bands implies the possible momentum shift of exciton ground states and the strain-reshaped exciton band structures.

Theoretically, the first theoretical research on the BX band structures of uni-axially strained MoS₂-MLs could be traced back to the pioneering work by Hongyi Yu *et al.*,^{2,47} which predicted the strain-induced splitting of BX doublet at zero momentum and crossings of longitudinal and transverse BX bands at finite momenta. Recently, M. M. Glazov *et al.* built up a strain-dependent model Hamiltonian for BXs in a WSe₂-ML under uni-axial strain according to the symmetry arguments and conducted the analysis for the strain-dependent BX fine structures.^{48,49} Yet, the excitonic effects of VD in uni-axially strained TMD-MLs, especially on

spin-forbidden GX and DX, have not been investigated and identified on the base of first principles, beyond those existing model studies.

In this work, we present a comprehensive theoretical investigation of the strain-modulated excitonic properties of uni-axially strained MoS₂-MLs by solving the Bethe-Salpeter equation (BSE) in the Wannier tight-binding scheme established on the basis of first principles. We show that imposing an uni-axial strain onto a MoS₂-ML results in diversified fine structures and band dispersions of BX, GX, and DX states, as a consequence of the competitive interplay between strain-induced VD and momentum-dependent *e-h* exchange interaction (EHEI). We show that the strain-diversified band dispersions, characterized by very distinct effective exciton masses, of BX, GX and DX makes it possible to not only *spectrally* but also *spatially* resolve BX, GX and DX in the exciton diffusive transport experiments or angle-resolved optical spectroscopy on uni-axially strained TMD-MLs.

Results and discussion

Electronic band structure

Figure 1 (a), (d) and (g) depict the lattice structures and the reciprocal Brillouin zones of a MoS₂-ML under a tensile uni-axial stress, no stress, and a compressive uni-axial stress, respectively, being the three major cases studied in this work. Throughout this work, we consider uni-axial stresses applied to a MoS₂-ML along the crystalline axis of zigzag atom chain, specified to be the *x*-axis. Figure 1 (b), (e), and (h) show the DFT-calculated quasi-particle band structures, $\epsilon_{n,\mathbf{k}}$ versus \mathbf{k} , of a MoS₂-ML under the tensile uni-axial stress, no stress, and compressive uni-axial stress along the *x*-axis, yielding the uni-axial strains, $\epsilon_{xx} = +5\%$, 0% , and -5% , respectively. Here, \mathbf{k} ($\epsilon_{n,\mathbf{k}}$) denotes the wave vector (eigenenergy) of Bloch states of electronic quasi-particles solved in the DFT. In the DFT-calculations, we consider the strain perpendicular to the uni-axial stress axis as well, which is given by $\epsilon_{yy} = -\sigma\epsilon_{xx}$, determined

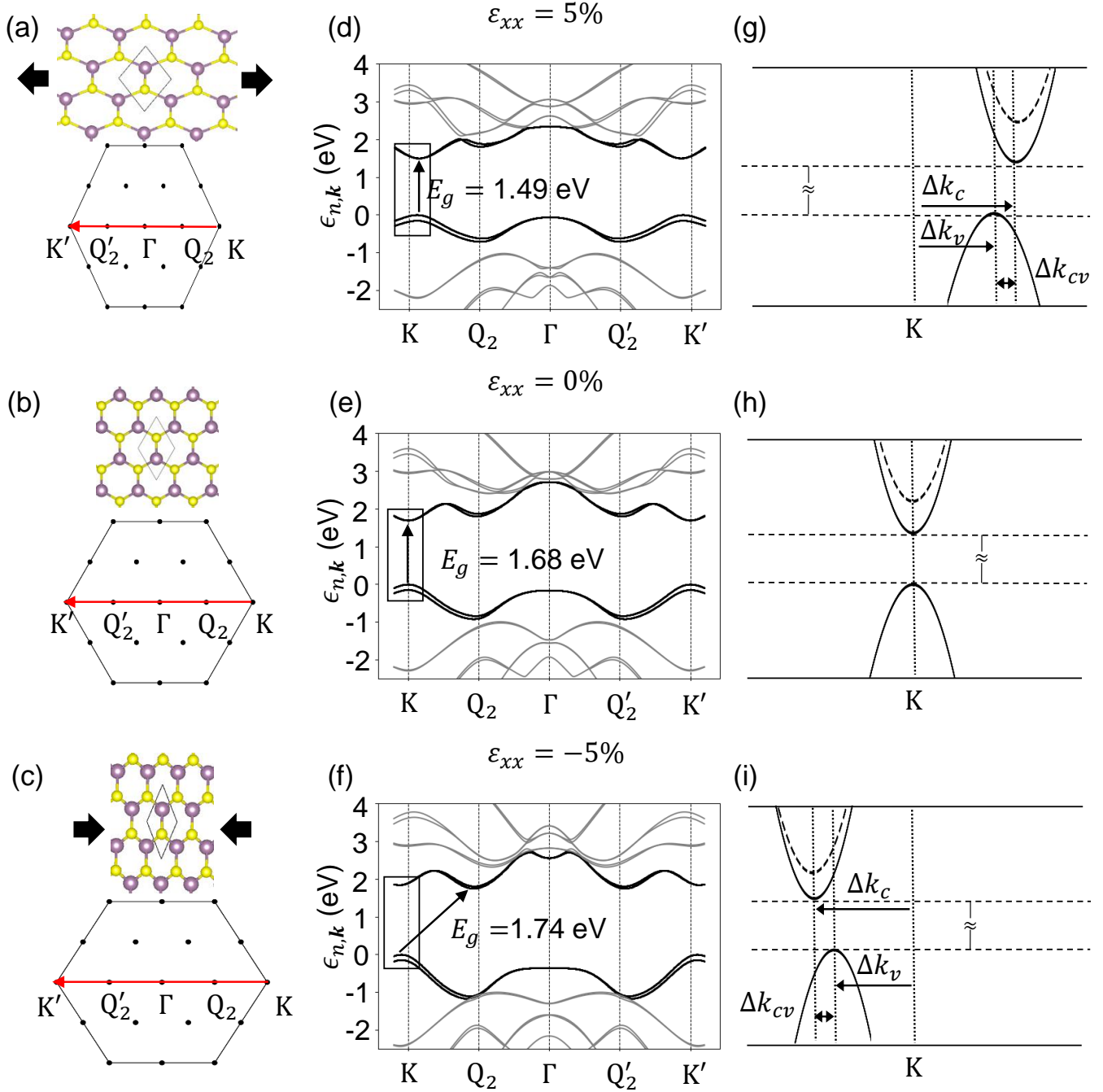


Figure 1: (a) Schematics of the lattice structures and reciprocal Brillouin zones of a MoS₂-ML with a tensile uni-axial strain ($\epsilon_{xx} > 0$) along the x-axis, where the x-axis is specified to be along the axis of zigzag atom chain of MoS₂-ML. (b) The DFT-calculated electronic band structures of a MoS₂-ML with the tensile uni-axial strain of $\epsilon_{xx} = 5\%$. (c) The zoom-in view of the conduction and valence bands of (b), around the K-valley. The solid (dashed) lines represent the up-spin (down-spin) bands. Δk_c (Δk_v) denotes the strain-induced VD of the conduction (valence) band. (d-f) [(g-i)] Same as (a-d) but for the un-strained [compressively strained] MoS₂-ML with $\epsilon_{xx} = 0\%$ [$\epsilon_{xx} = -5\%$].

by the Poisson's ratio, $\sigma = 0.31$, of MoS₂-ML.⁵⁰ More technical information of the DFT calculation for strained MoS₂-MLs is detailed in Sec. I.A of Supporting Information (SI).

In Figure 1 (b), (e) and (h), it is shown that, with varying $\varepsilon_{xx} = 5\%$, $\varepsilon_{xx} = 0\%$ to $\varepsilon_{xx} = -5\%$, the energy gap of the strained MoS₂-ML increases from $E_g = 1.49\text{eV}$, $E_g = 1.68\text{eV}$, to $E_g = 1.75\text{eV}$, and transits from an intra-valley (K-K) energy gap to an inter-valley (K-Q) indirect gap. Without employing the GW method,⁵¹⁻⁵⁴ the calculated band gaps in the DFT are underestimated as compared with experimental values.^{1,55} Nevertheless, the predicted strain-dependent electronic and excitonic structures of MoS₂-MLs by the DFT with the commonly used PBE functional are sufficiently valid and useful for the physical investigation under the scope of this work.

Figure 1 (c), (f) and (i) shows the zoom-in views of the conduction and valence bands of the uni-axially strained MoS₂-ML around the K valley, showing the VD inwards (outwards) the center of the Brillouin zone under an imposed tensile (compressive) uni-axial strain. With $\varepsilon_{xx} = 5\%$, the calculated drift of the conduction (valence) valley is $\Delta k_c = 0.091\text{\AA}^{-1} = 94.8Q_c$ ($\Delta k_v = 0.074\text{\AA}^{-1} = 76.8Q_c$), two orders of magnitude larger than the wave vector of light cone (LC) edge, $Q_c \equiv \frac{E_{S,0}^X}{\hbar c} \approx 9.6 \times 10^{-4}\text{\AA}^{-1}$, where \hbar denotes the Planck's constant, c the speed of light in vacuum, and $E_{S,0}^X \approx 1.9\text{eV}$ is estimated by the DFT-BSE-calculated exciton energy.⁵⁶ Nowadays, it has been established that such uni-axial strain-induced VDs^{42-44,57} are essential in non-linear topological physics and valley magnetization.^{40,41,45,46,58,59}

Note that the strain-induced VDs of conduction and valence bands are towards the same direction but differ in the magnitude, i.e. $\Delta k_c \neq \Delta k_v$ for a fixed strain. The difference between the strain-induced conduction- and valence-VDs is approximately $3Q_c/\%$, implying the significant momentum shifting of exciton band. Naively disregarding the Coulomb interaction of exciton, the lowest excited states of a uni-axially strained TMD-ML should be the momentum-forbidden DX states with a large

exciton wave vector, $Q = \Delta k_c - \Delta k_v \equiv \Delta k_{cv}$, out of the LC. However, as we shall show later, the competitive interplay between the VD and momentum-dependent EHEI leads to the diversified band dispersions of BX, GX and DX of an uni-axially strained TMD-ML, generally deviating from the naive non-interacting scenario.

Exciton band dispersions

Based on the DFT-calculated electronic band structures, we proceed with the calculations of the fine structures and band dispersions of 1s exciton of the un-strained and strained MoS₂-MLs by employing the developed computational methodology in Refs. 12,60. For a 2D material system, the states of exciton are characterized by the in-plane wave vector in the center-of-mass coordinate, $\mathbf{Q} = (Q_x, Q_y)$, and labelled by the symbol $S=(B_u, B_l, GX, DX)$ to denote the type of exciton. The eigenenergy, $E_{S,\mathbf{Q}}^X$, of a exciton state, $|S, \mathbf{Q}\rangle$, which carry the center-of-mass momentum, $\hbar\mathbf{Q}$, is obtained by solving the DFT-based BSE. Figure 2 presents the calculated low-lying band dispersions, $E_{S,\mathbf{Q}}^X$, of exciton, including the longitudinal (L) upper bands and transverse (T) lower bands of BX (denoted by B_u and B_l , respectively), and those of spin-forbidden GX and DX, of un-strained and strained hBN-encapsulated MoS₂-MLs with $\varepsilon_{xx} = +5\%$, $\varepsilon_{xx} = 0\%$, $\varepsilon_{xx} = -5\%$, respectively, versus \mathbf{Q} parallel (Figure 2 (a),(c) and (e)) or perpendicular (Figure 2 (b),(d) and (f)) to the uni-axial stress axis.

Throughout this work, we consider the hBN-sandwiched MoS₂-MLs as depicted in the inset of Figure 2. The non-local Coulomb screening in the multi-layer system is evaluated and considered in the BSE following the electrostatic theory used in Ref. 12 for quantitative simulation of hBN-encapsulated TMD-MLs.⁶¹⁻⁶⁴ For more details of the employed BSE theory and computational methodology, one can refer to the SI and Ref. 60.

Un-strained MoS₂-ML

The calculated exciton fine structure of un-strained MoS₂-ML as shown in Figure 2 (c)

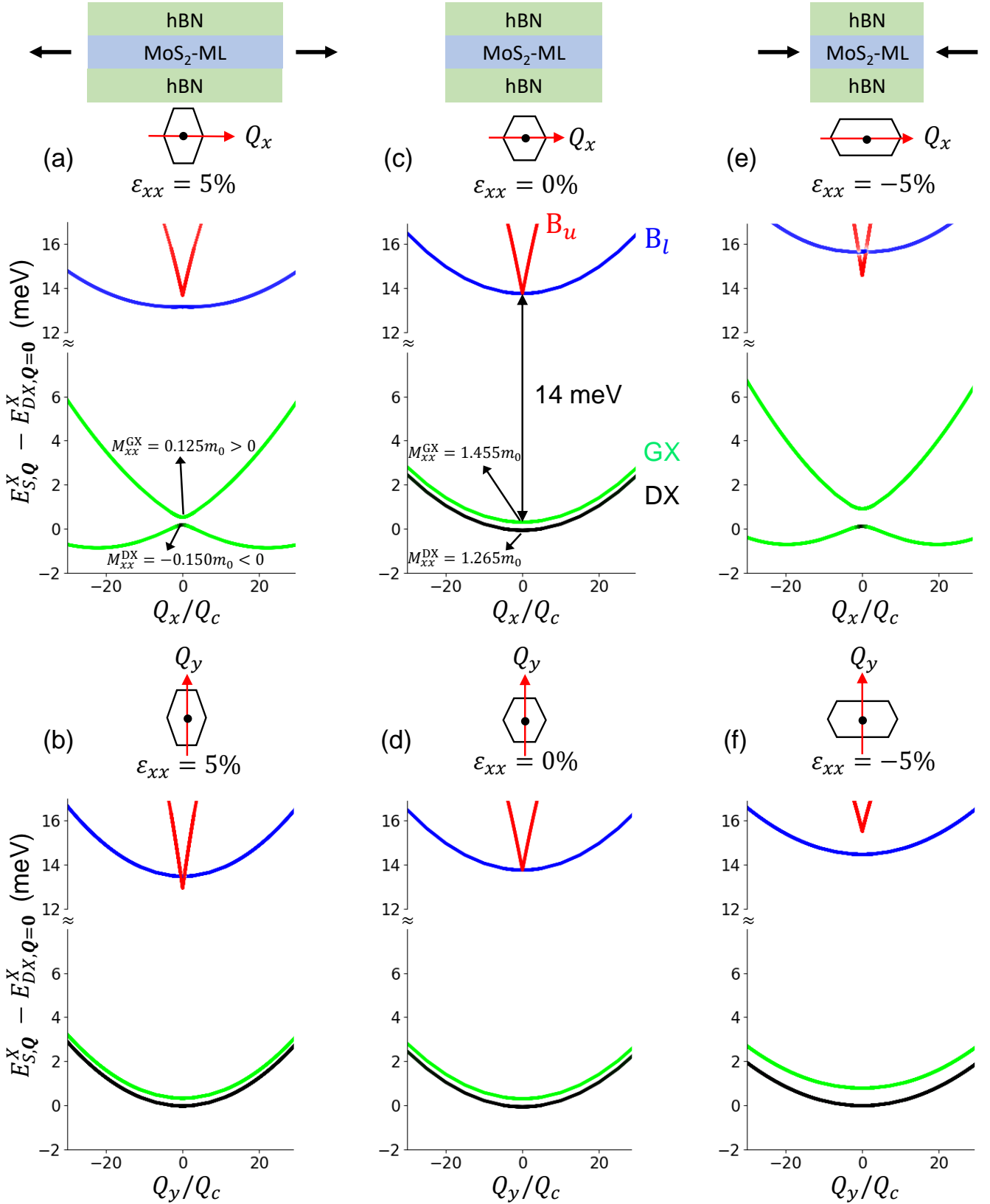


Figure 2: (a-b) Fine structure in the energy bands of BX, GX and DX in a strained MoS₂-ML with the tensile uni-axial strain, $\epsilon_{xx} = +5\%$, along (a) Q_x -axis (b) Q_y -axis. The BX doublet is split by EHEI into the upper and lower bands, denoted by B_u and B_l , respectively. The grading of red (blue) color represents the magnitude of longitudinal (transverse) transition dipoles. The grading of the color from dark to green represents the magnitude of the out-of-plane dipole of exciton. Inset: Schematic of the hBN-sandwiched MoS₂-MLs. (c-d) Same as (a-b) but for the un-strained MoS₂-ML. (e-f) Same as (a-b) but for the compressive uni-axial strain MoS₂-ML.

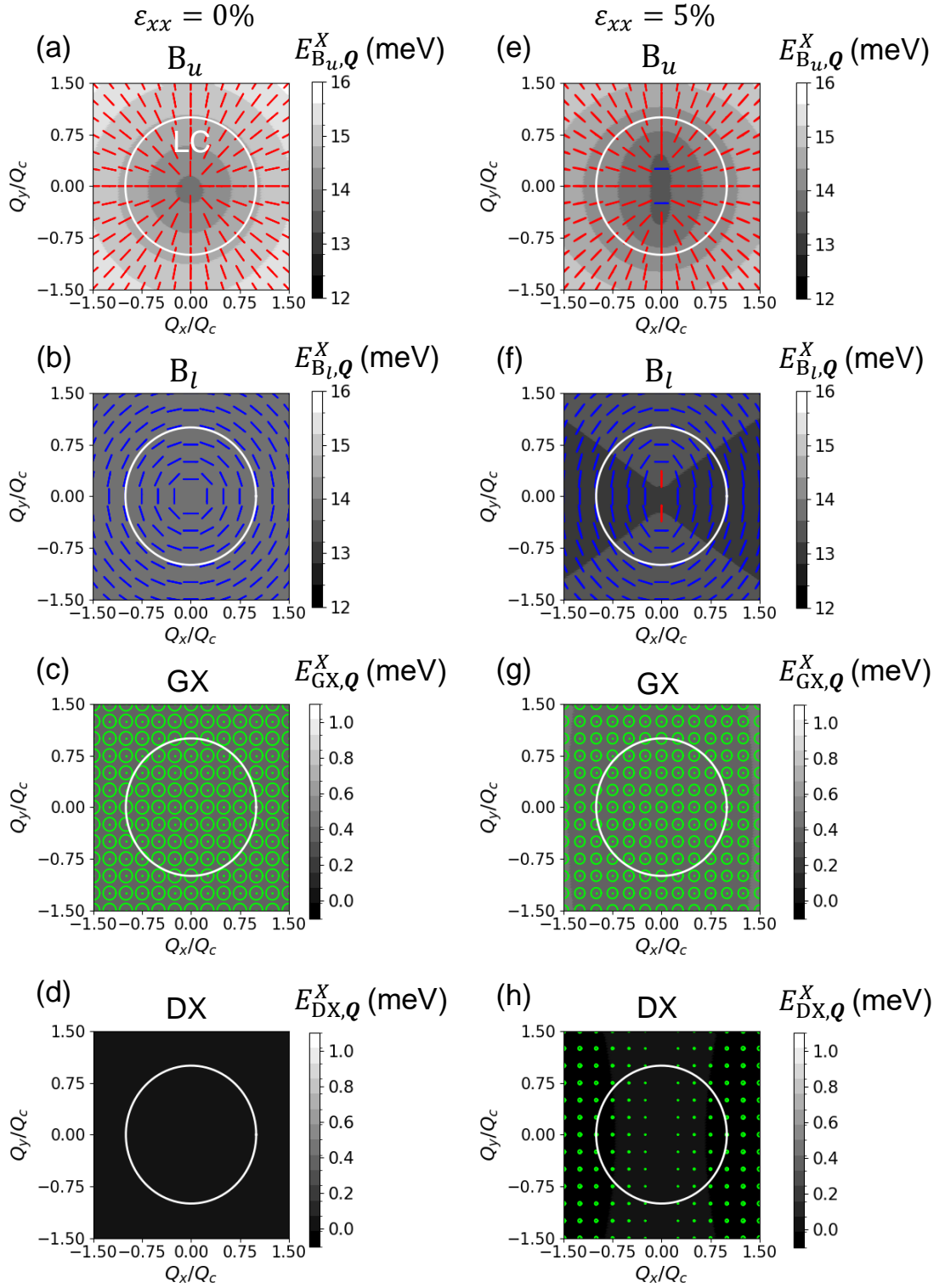


Figure 3: (a-d): The energy contours of the B_u , B_l , GX, and DX bands of an un-strained MoS_2 -ML with $\epsilon_{xx} = 0\%$. The red (blue) line segments placed in the \mathbf{Q} -plane represent the magnitudes and orientations of the longitudinal (transverse) dipoles of the BX states with \mathbf{Q} . The size of green circle represents the magnitude of out-of-plane dipole of GX and DX states. (e-h): Same as (a-d) but for a uni-axially strained MoS_2 -ML with $\epsilon_{xx} = 5\%$. The large white circle indicates the boundary of LC where $Q = Q_c$.

and (d) exhibits the BX-DX splitting of 14 meV, which is in excellent agreement with the experimental observation of Ref. 62. As recognized from the previous studies, the BX-DX splitting results from the combined effects of spin-orbit interaction and Coulomb interactions^{12,65,66} For MoS₂-MLs, the latter effect contributes the dominant short-ranged EHEI (SR-EHEI) to push upwards the energies of the spin-allowed BX doublet and leave the spin-forbidden exciton one (GX and DX) to be the lowest exciton states. The similar dispersive features of Figure 2 (c) to that of Figure 2 (d) indicates the nearly isotropic exciton band structure of an un-strained MoS₂-ML, as observed in the exciton energy contours of Figure 3 (a)-(d).

In the absence of strain, it is known that the BX bands are doubly valley-degenerate at the Γ_{ex} point where $\mathbf{Q} = (0, 0)$ and, with increasing $|\mathbf{Q}| \neq 0$, turn out to be split by the long-ranged EHEI (LR-EHEI)^{47,66}. Note that the upper B_u-band exhibits a quasi-linear dispersion due to the nature of dipole-dipole interaction in the LR-EHEI.^{47,60,66} As the result of LR-EHEI, the BX states in the linear B_u-band (parabolic B_l-band) carry the longitudinal (transverse) in-plane dipoles whose orientation are aligned (perpendicular) to the exciton momentum. Figure 3 presents the momentum-dependent transition dipoles of excitons, $\mathbf{D}_{S,\mathbf{Q}}^X$, in a un-strained and strained MoS₂-MLs, which are calculated by using the DFT-based exciton theory that is detailed in Sec.I.C of SI.^{60,67,68}

The SR-EHEI leads to a tiny sub-nm-scaled splitting of the spin-forbidden exciton doublet, and, combined with the spin-orbit interaction, activates the brightness of upper spin-forbidden states with small out-of-plane dipoles.¹¹ Hence, the upper band of the DX doublet is often referred to as GX band. Figure 3 (c) shows the out-of-plane dipoles of the finite-momentum GX states of an un-strained MoS₂-ML. Note that, by contrast to the optical activation of the upper GX band, the lower DX band still remain totally dark in a strain-free MoS₂-ML.

Strained MoS₂-ML

Figure 2 (a) and (b) show the calculated exciton band dispersions of a MoS₂-ML under a fixed tensile uni-axial strain of $\varepsilon_{xx} = +5\%$ with respect to \mathbf{Q} along the x - and y -axes, respectively. Unlike the un-strained case, Figure 2 (a) and (b) exhibit distinct exciton band dispersions, indicating the strain-induced anisotropy of the exciton band structure. First, one notes that, under the tensile uni-axial strain, the parabolic transverse (blue curve) band and the linear longitudinal (red curve) one of BX no longer remain degenerate at the Γ_{ex} point, as previously pointed out in the literature.^{35,37,49}

Note that, in a non-interacting scheme, the strain-induced unequal conduction and valence VDs (as shown in Figure 1 (c)) tends to lower the energy of finite-momentum exciton with increasing the $Q(\leq Q_c < \Delta k_{cv})$ in the LC. Despite VD-induced $\Delta k_{cv} \neq 0$, we find that the lowest BX states of a strained MoS₂-ML stay at the Γ_{ex} point, without momentum drift actually. This is because tightly bound BXs in a 2D material are own large in-plane dipoles and are subjected to the strong momentum-dependent EHEI that overwhelms the kinetic valley drift to dictate the exciton dispersions.

In contrast to spin-allowed BXs, our first principles studies reveal that an imposed uni-axial stress directly impacts the spin-forbidden exciton states in both the band dispersions as well as the optical selection rules. In Figure 2 (a), one notes that the curvature of the upper parabolic GX band along the Q_x -axis is significantly increased by the tensile uni-axial strain. It turns out that the effective mass of GX along the x -axis is dropped from $M_{xx}^{GX} = 1.455m_0$ to $0.125m_0$, by one order of magnitude, with varying the uni-axial strain from $\varepsilon_{xx} = 0\%$ to $+5\%$, where the exciton mass is defined by $M_{ij}^S \equiv \left(\frac{1}{\hbar^2} \frac{\partial^2}{\partial Q_i \partial Q_j} E_{S,\mathbf{Q}}^X \right)^{-1} \Big|_{\mathbf{Q}=\mathbf{0}}$, and $m_0 = 9.1 \times 10^{-31}$ kg is the mass of free electron.

Even more interestingly, the lower DX band under the dictating effect of VD is drastically reshaped by the imposed tensile uni-axial strain from a parabola to a Mexican-hat-like dispersion, featured with the finite-momentum exciton ground states and the sign-reversed effective mass, $M_{xx}^{DX} = -0.150m_0 < 0$, at the Γ_{ex} -

point. Notably, applying an uni-axial strain on a TMD-ML is found to give rise to very small out-of-plane dipoles and weak brightnesses onto the spin-forbidden DX states with finite Q_x , as shown in Figure 3 (h). Because the strain-induced dipoles of the DX states are extremely small, the strain-induced kinetic VD overwhelms the nearly vanishing EHEI and dictates the finite-momentum DX to form the unusual Mexican-hat-like dispersion featured by the exciton ground states with $|\mathbf{Q}| \equiv Q_0 \sim 21.5Q_c$. Despite $Q_0 \gg Q_c$, Q_0 falls in the sub-wavelength regime accessible in nano-optics, such as plasmonic radiation or non-radiative dipole-dipole interaction in energy transfer.^{65,69,70} This suggests the emergent importance of DX in nano-optics based on strained 2D materials.

Now, let us turn to examine the the exciton band structure of a MoS₂-ML under compressive uni-axial strain, as shown in Figure 2 (e) and (f). Comparing Figure 2 (e) and (f) with Figure 2 (a) and (b), one sees that the exciton band structure of a MoS₂-ML with compressive strain is quite similar to that with tensile strain, except for the reversed order of the transverse and longitudinal BX bands. Such a similarity in the exciton band structures is not too surprised, since, due to the Poisson's ratio, applying a compressive uni-axial strain to a 2D material along the x -axis induces also another tensile uni-axial strain along the y -direction perpendicular to the uni-axial strain axis. Thus, hereafter we shall focus the investigation only on the MoS₂-MLs with tensile uni-axial strains to reduce the repetition of physical analysis.

Strain-modulated exciton dipoles and band energy contours

Figure 3 (a-d) [(e-h)] present the energy contour plots of the calculated exciton bands ($E_{B_u, \mathbf{Q}}^X$, $E_{B_l, \mathbf{Q}}^X$, $E_{GX, \mathbf{Q}}^X$, and $E_{DX, \mathbf{Q}}^X$, respectively) of BX doublet, GX, and DX of the MoS₂-MLs without strain [with tensile strain]. The transition dipole, $D_{S\mathbf{Q}}^X$, of an exciton state with the momentum $\hbar\mathbf{Q}$ is presented by a line segment (representing a linearly polarized dipole) or a circle (representing a circularly polarized out-of-

plane dipole) placed at the position of \mathbf{Q} in the momentum plane, whose size and orientation reflect the magnitude and orientation of dipole, respectively. In the absence of strain, all exciton bands of an un-strained MoS₂-ML remain nearly isotropic, and each finite momentum exciton states hold well-defined longitudinal, transverse, or out-of-plane dipoles (represented in red, blue, and green colors, respectively, in Figure 3 (a-c)). Since the lowest DX band of an un-strained MoS₂-ML are optically completely dark, no symbol of dipole appear in Figure 3 (d).

Under the uni-axial strain, the energy contours of the BX upper and lower bands are deformed to be anisotropic, as shown in Figure 3 (e) and (f). By contrast, the GX band interestingly remains nearly isotropic against the uni-axial strain, as seen in Figure 3 (g). In Figure 3 (h), we see that the DX states with finite momenta around the direction along the stress-axis surprisingly exhibit the strain-induced out-of-plane dipoles, leading to a weak brightness and indicating the violation of the spin selection rule for DX. The strain-induced optical brightness in the DX states results from the symmetry breaking caused by the uni-axial strain, as shown by Ref. 71, which acts as an effective longitudinal magnetic field that couples the DX to the GX states with small out-of-plane dipoles.⁷¹

Strain-diversified exciton masses

From the DFT-based studies, we realize that the different types of excitons in a uni-axially strained MoS₂-ML follow the diversified band dispersions, characterized with the strain-modulated effective masses of exciton, M_{ij}^S . The exciton effective mass has been known as a key parameter to determine the steady exciton diffusivity in exciton transport.^{16,72-78} Following the studies of Refs. 72-75, the directional steady diffusivity of exciton is quantified by the diffusion coefficient \mathbf{D}^{diff} whose elements are proportional to the inverse exciton effective mass, *i.e.*, $D_{ij}^{\text{diff}} \propto (M_{ij}^S)^{-1}$, $i, j = x$ or y .

Figure 4 (a) presents the strain-dependences of the effective masses of exciton along the uni-axial strain axis, M_{xx}^S , for BX, GX, and DX

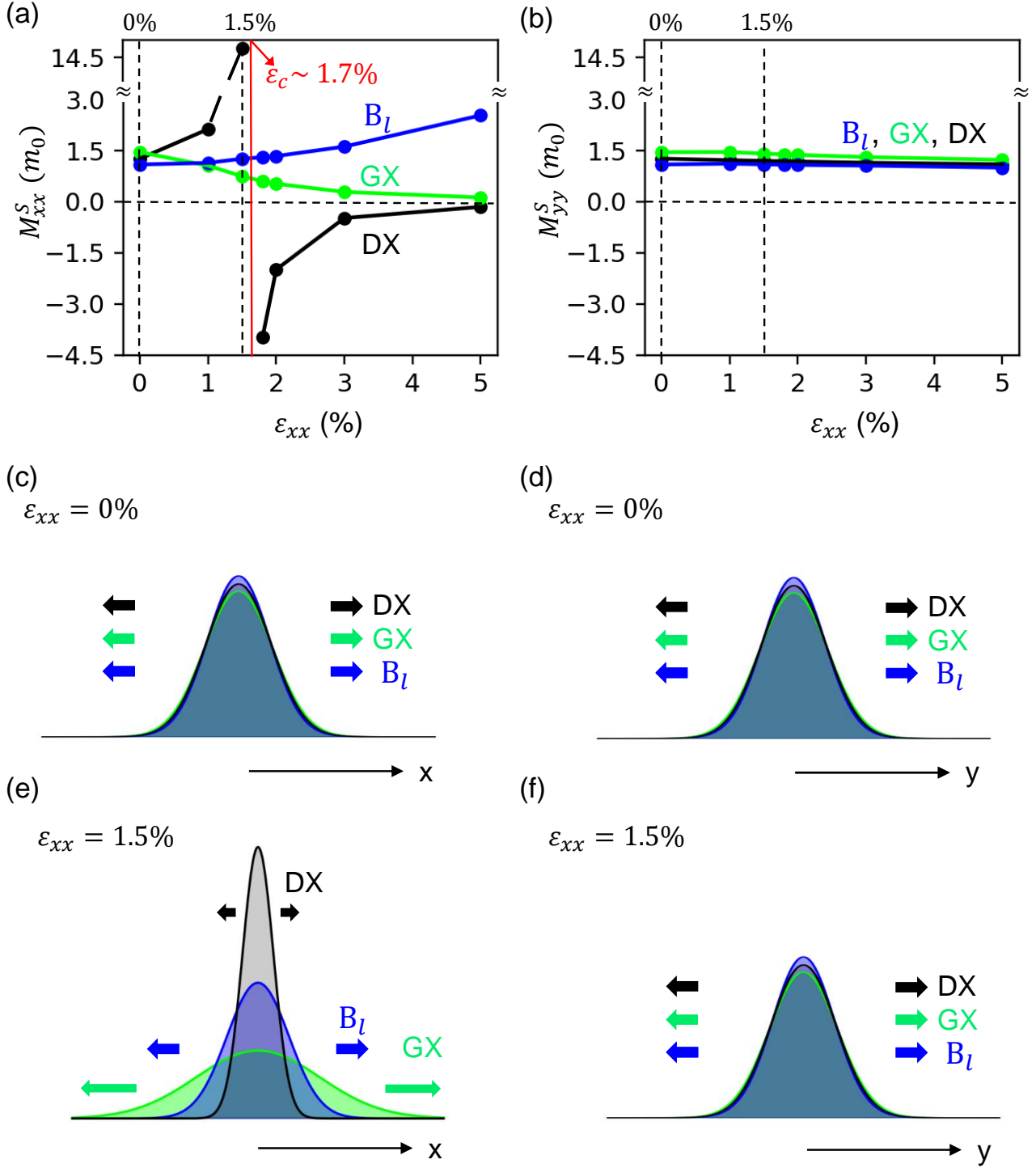


Figure 4: (a) [(b)] The strain-modulated effective masses, M_{xx}^S [M_{yy}^S], of BX (blue curve), GX (green curve), and DX (black curve) along the x -axis [y -axis] of a MoS₂-ML under the uni-axial strain varied from $\epsilon_{xx} = 0\%$ to $\epsilon_{xx} = +5\%$. (c) [(d)] Schematics of exciton diffusion of BX, GX and DX in an unstrained MoS₂-ML, propagating along the x -direction [y -direction] with similar diffusive lengths. (e) [(f)] Schematics of exciton diffusion of BX, GX and DX in an uni-axially strained MoS₂-ML with $\epsilon_{xx} = 1.5\%$, along the x -direction [y -direction] with diversified [similar] diffusive lengths.

($S = B_l, GX, \text{ and } DX$) in a strained MoS_2 -ML with varying the tensile uni-axial strain, which are shown very diversified especially around the critical strain ϵ_c . With increasing the uni-axial strain from $\epsilon_{xx} = 0\%$ up to $\epsilon_{xx} = +5\%$, one sees that the $M_{xx}^{B_l}$ of BX gradually increases from $1.094m_0$ to $2.535m_0$ but, oppositely, the M_{xx}^{GX} of GX decreases drastically from $1.455m_0$ down to $0.125m_0$. The presence of uni-axial strain is shown to impact most the M_{xx}^{DX} of DX as presented by the black curve in Figure 4 (a). With increasing ϵ_{xx} , M_{xx}^{DX} quickly increases but abruptly reverses its sign to become negative at the critical strain $\epsilon_{xx} \approx 1.7\% \equiv \epsilon_c$, where the Mexican-hat-like band dispersion emerges. With the strain greater than ϵ_c , the negative M_{xx}^{DX} yet turns out to decrease its magnitude. The non-monotonic strain-dependence of M_{xx}^{DX} results from the emergence of the unusual strain-induced Mexican-hat-like dispersion, manifesting the pronounced excitonic effect of VD on the spin-forbidden exciton.

By contrast to strain-diversified exciton masses along the x -direction, M_{xx}^S , the effective masses of exciton along the y -axis, M_{yy}^S , remain almost unchanged against varied ϵ_{xx} , as one sees in Figure 4 (b). This indicates the strain-insensitive exciton diffusion along the direction perpendicular to the axis of uni-axial strain, and the strain-induced anisotropy in the exciton diffusivity. Along the uni-axial strain axis, the strain-diversified exciton masses, M_{xx}^S , of a uni-axially strained TMD-ML should lead to distinct diffusion lengths of BX, GX, and DX, especially as $\epsilon_{xx} \sim \epsilon_c$, as schematically shown by Figure 4 (e). Accordingly, one can infer that a GX in a uni-axially strained MoS_2 -ML should exhibit a high diffusivity because of the strain-reduced mass of GX. By contrast, the drastically increased M_{xx}^{DX} especially as $\epsilon_{xx} \sim \epsilon_c$ suggests the low diffusivity and strain-stabilized localization. The predicted diversification in the effective masses of exciton reveals the possibility to spatially resolve the BX, GX, and DX in exciton transport experiments by means of imposing an uni-axial strain to a TMD-ML.

Angle-resolved photoluminescence spectra

The strain-induced diversification and anisotropies in the exciton band structures of BX, GX, and DX leads also to the diversified angle-dependences of the directional photoluminescences (PLs) from the different types of exciton in an uni-axially strained MoS_2 -ML. Based on the DFT-BSE-solved exciton states and momentum-dependent transition dipoles of BX, GX, and DX, we calculate the transition rates of the directional PLs from an exciton in an uni-axially strained MoS_2 -ML, as a function of the polar (θ_ν) and azimuthal (ϕ_ν) angles of the emitted light. The technical details of the calculations for the directional PLs are presented in Sec. II of SI.

Figure 5 shows the optical patterns of the directional PLs, characterized by the momentum-dependent transition rates of exciton, $\Gamma_{S,Q}(\theta_\nu, \phi_\nu)$, from the exciton states of un-strained and uni-axially strained MoS_2 -MLs. Figure 5 (a-d) present the optical patterns of the $B_u, B_l, GX, \text{ and } DX$ bands of an un-strained MoS_2 -ML, all of which present isotropic features. In the presence of uni-axial strain, the optical patterns of the BX states of an uni-axially strained MoS_2 -ML turn out to be anisotropic, as shown by Figure 5 (g) and (h). By contrast to the BX states, the optical pattern of the GX states of a uni-axially strained MoS_2 -ML yet is found strain-insensitive and presents only slight anisotropy as one sees in Figure 5 (i). Interestingly, we show that the optical pattern of the DX states exhibit the most anisotropy (See Figure 5 (j)). The strain-induced small brightness of DX yields the weak directional light emission that tends to propagate in the direction around the x -axis, nearly horizontally with large polar angle. The large-polar-angle directional light emission from the long-lived spin-forbidden DXs in a uni-axially strained MoS_2 -ML could be considered as a signature of strain-induced excitonic effect of VD, optically measurable in the time- and angle-resolved optical spectroscopy.

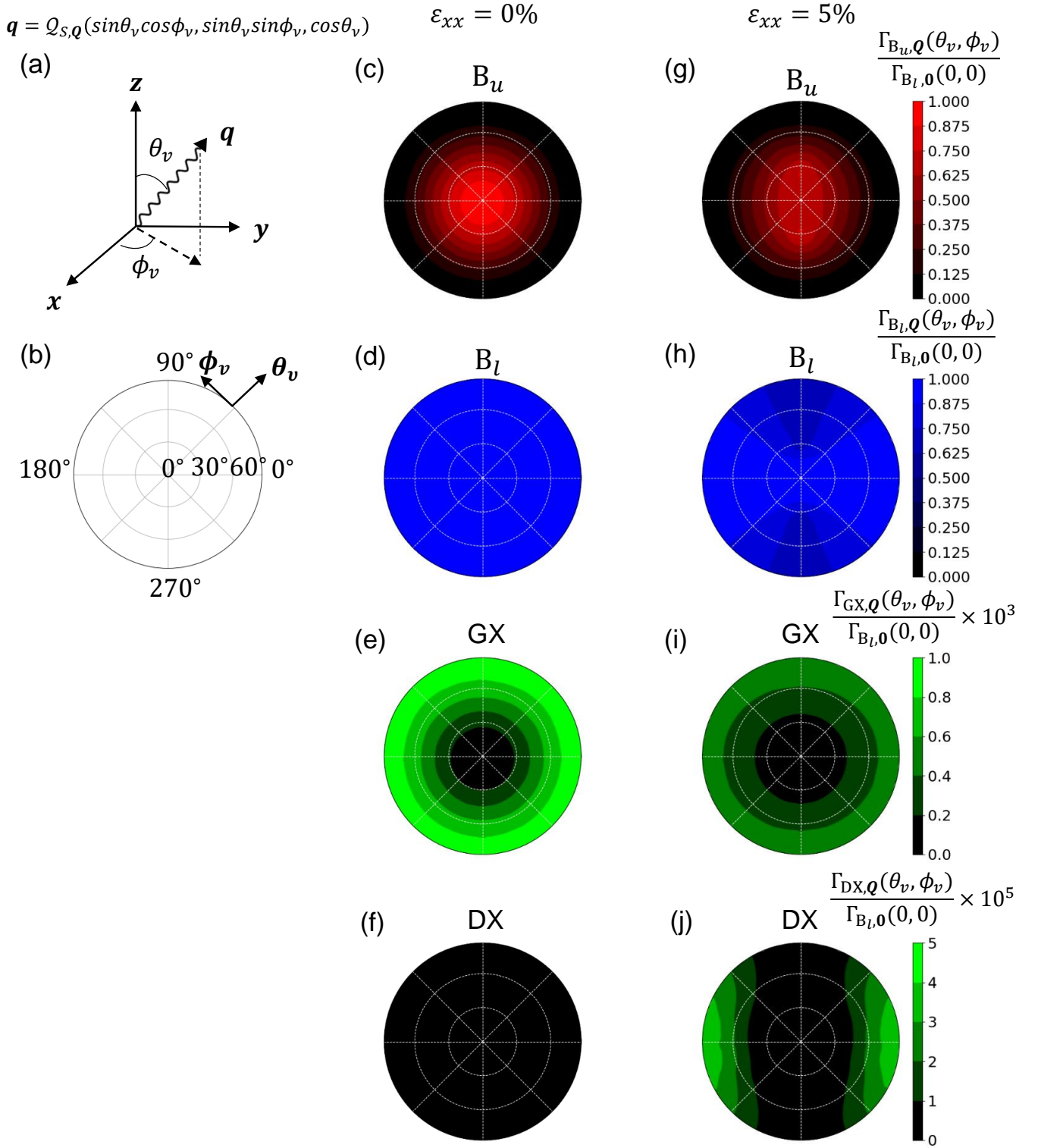


Figure 5: (a) Schematics of a directional light beam of PL with the polar angle, θ_ν , and the azimuthal angle, ϕ_ν , in the spherical coordinate, and $Q_{S,\mathbf{Q}} = \frac{E_{S,\mathbf{Q}}^X}{\hbar c}$ represents the magnitude of the wave vector of the emitted light. (b) The top view for a hemisphere, where the radius of circle represents θ_ν and the azimuthal angle represents ϕ_ν . (c-f) The θ_ν - and ϕ_ν -resolved optical patterns of the relative transition rates, $\Gamma_{S,\mathbf{Q}}^S(\theta_\nu, \phi_\nu)/\Gamma_{B_l,0}^S(0,0)$, of the directional PLs from the B_u , B_l , GX , and DX exciton states, respectively, of an un-strained MoS_2 -ML. (g-j) The angle-resolved optical patterns of the four types of exciton states of an uni-axially strained MoS_2 -ML with $\varepsilon_{xx} = 5\%$.

Conclusions

In summary, we have presented a comprehensive theoretical investigation of the strain-modulated excitonic fine structures and band dispersions of uni-axially strained MoS₂-MLs by solving the first-principles-based BSE. As a main finding, imposing an uni-axial strain onto a MoS₂-MLs significantly diversifies the band dispersions, diffusive transport properties, and angle-resolved optical patterns of the BX, GX, and DX states, as a consequence of the competitive interplay between the strain-induced VD and momentum-dependent EHEI. We show that, while the band dispersions of BX doublet remain almost unchanged against strain, the presence of an uni-axial strain in a MoS₂-ML impacts most the spin-forbidden exciton states, both GX and DX. Imposing only a few-percentage uni-axial strain onto a MoS₂-ML can reshape the band dispersion of DX states from a parabola to a Mexican-hat-like profile, featured with strain-activated brightness and abrupt sign-reversal of the effective mass of DX. Oppositely, the band dispersion of GX in a uni-axial strained MoS₂-ML that remain parabolic is featured by a drastically strain-reduced effective mass. The strain-induced diversification in the exciton band dispersions of a uni-axial strained MoS₂-ML is shown to diversify and make very distinct the diffusive lengths and angle-resolved optical patterns of BX, GX, and DX as well, as the measureable signatures of strain-induced VD. This suggests the possibility of not only *spectrally* but also *spatially* resolving the BX, GX and DX exciton states of a uni-axially strained 2D material in exciton diffusive transport experiments or the angle-resolved optical spectroscopy.

Methods

DFT and BSE calculations

We calculated the quasi-particle band structures and wave functions of strained MoS₂-ML by utilizing the Quantum Espresso (QE) package.⁷⁹ In the DFT calculations, we considered the un-strained MoS₂-ML with lattice

constant $a_0 = 3.16\text{\AA}$. We employed $15 \times 15 \times 1$ Monkhorst-Pack k-grid to ensure the convergence of our calculation. We chose the Perdew-Burke-Ernzerhof (PBE) exchange-correlation functional⁸⁰ and used norm-conserving pseudopotential taking into account the relativistic effects. The plane-wave cutoff was set to be 70 Ry. In the technical implementation of the DFT-simulation for a 2D MoS₂-ML, we set the vacuum between periodic layers to be larger than 30 \AA . For strained MoS₂-MLs, we consider the effect of Poisson's ratio but neglect the small out-of-plane strain.

For raising up the efficiency of DFT-based BSE calculation, we transformed the set of DFT-calculated quasi-particle wave functions to the maximally localized Wannier functions (MLWFs) by utilizing the WANNIER90 package,⁸¹ and, in the basis of MLWFs, established the DFT-based BSE in the Wannier tight binding scheme, which is beneficial to save the numerical time. Then, we calculated the exciton fine structures and band dispersions of hBN-encapsulated MoS₂-ML by utilizing our in-house code to solve the DFT-based BSE with the consideration of the non-local dielectric screening in the multi-layer system.^{12,60,82} For more technical details, one can refer to the SI.

ASSOCIATED CONTENT

Supporting Information

Technical details on establishing the Bethe-Salpeter equation based on first-principles; guidelines for evaluating the transition dipole of an exciton; formalisms for angle-resolved photoluminescence spectra.

Author Contributions

S.-J.C. and C.-H.C. conceived the project. S.-J.C. supervised the project. C.-H.S., G.-H.P., and M.-L.X. carried out the DFT-calculations. C.-H.S., P.-Y.L., and W.-H.L. carried out the BSE calculations. C.-H.S. and G.-H.P. performed angle-resolved PL spectra simulations. C.-H.S. and S.-J.C. wrote the paper with input

from other authors. All authors participated in discussions and revisions of the manuscript.

Notes

The authors declare no competing financial interest.

ACKNOWLEDGMENTS

C.H.C.

This work is financially supported by the National Science and Technology Council (NSTC), Taiwan, T-Star center project “Future Semiconductor Technology Research Center”, under Grant No. NSTC 113-2634-F-A49-008.

S.J.C.

The research study is supported financially by the NSTC of Taiwan (Grant Nos. NSTC 112-2112-M-A49-019-MY3, NSTC 112-2622-M-A49-001, NSTC 113-2112-M-A49-035-MY3, and NSTC 113-2124-M-A49-008). The authors thank the National Center for High-Performance Computing (NCHC) in Taiwan for providing computational resources.

References

- (1) Mak, K. F.; Lee, C.; Hone, J.; Shan, J.; Heinz, T. F. Atomically Thin MoS₂: A New Direct-Gap Semiconductor. *Phys. Rev. Lett.* **2010**, *105*, 136805.
- (2) Yu, H.; Cui, X.; Xu, X.; Yao, W. Valley excitons in two-dimensional semiconductors. *Natl. Sci. Rev.* **2015**, *2*, 57–70.
- (3) Zeng, H.; Dai, J.; Yao, W.; Xiao, D.; Cui, X. Valley polarization in MoS₂ monolayers by optical pumping. *Nat. Nanotechnol.* **2012**, *7*, 490–493.
- (4) Kumar, A. M. et al. Strain fingerprinting of exciton valley character in 2D semiconductors. *Nat. Commun.* **2024**, *15*, 7546.
- (5) Gupta, G.; Watanabe, K.; Taniguchi, T.; Majumdar, K. Observation of ~100% valley-coherent excitons in monolayer MoS₂ through giant enhancement of valley coherence time. *Light: Sci. Appl.* **2023**, *12*, 173.
- (6) Ugeda, M. M.; Bradley, A. J.; Shi, S.-F.; da Jornada, F. H.; Zhang, Y.; Qiu, D. Y.; Ruan, W.; Mo, S.-K.; Hussain, Z.; Shen, Z.-X.; Wang, F.; Louie, S. G.; Crommie, M. F. Giant bandgap renormalization and excitonic effects in a monolayer transition metal dichalcogenide semiconductor. *Nat. Mater.* **2014**, *13*, 1091–1095.
- (7) Li, Z. et al. Momentum-Dark Intervalley Exciton in Monolayer Tungsten Diselenide Brightened via Chiral Phonon. *ACS Nano* **2019**, *13*, 14107–14113, PMID: 31765125.
- (8) Bieniek, M.; Szulakowska, L.; Hawrylak, P. Band nesting and exciton spectrum in monolayer MoS₂. *Phys. Rev. B* **2020**, *101*, 125423.
- (9) Wu, F.; Qu, F.; MacDonald, A. H. Exciton band structure of monolayer MoS₂. *Phys. Rev. B* **2015**, *91*, 075310.
- (10) Bieniek, M.; Sadecka, K.; Szulakowska, L.; Hawrylak, P. Theory of Excitons in Atomically Thin Semiconductors: Tight-Binding Approach. *Nanomaterials* **2022**, *12*.
- (11) Echeverry, J. P.; Urbaszek, B.; Amand, T.; Marie, X.; Gerber, I. C. Splitting between bright and dark excitons in transition metal dichalcogenide monolayers. *Phys. Rev. B* **2016**, *93*, 121107.
- (12) Li, W.-H.; Lin, J.-D.; Lo, P.-Y.; Peng, G.-H.; Hei, C.-Y.; Chen, S.-Y.; Cheng, S.-J. The Key Role of Non-Local Screening in the Environment-Insensitive Exciton Fine Structures of Transition-Metal Dichalcogenide Monolayers. *Nanomaterials* **2023**, *13*.
- (13) Chen, Y.-H. et al. Efficient light upconversion via resonant exciton-exciton annihilation of dark excitons in few-layer transition metal dichalcogenides. 2024; <https://arxiv.org/abs/2409.03387>.

- (14) Liu, E.; van Baren, J.; Taniguchi, T.; Watanabe, K.; Chang, Y.-C.; Lui, C. H. Landau-Quantized Excitonic Absorption and Luminescence in a Monolayer Valley Semiconductor. *Phys. Rev. Lett.* **2020**, *124*, 097401.
- (15) Liu, E.; van Baren, J.; Liang, C.-T.; Taniguchi, T.; Watanabe, K.; Gabor, N. M.; Chang, Y.-C.; Lui, C. H. Multipath Optical Recombination of Intervalley Dark Excitons and Trions in Monolayer WSe₂. *Phys. Rev. Lett.* **2020**, *124*, 196802.
- (16) Uddin, S. Z.; Kim, H.; Lorenzon, M.; Yeh, M.; Lien, D.-H.; Barnard, E. S.; Htoon, H.; Weber-Bargioni, A.; Javey, A. Neutral Exciton Diffusion in Monolayer MoS₂. *ACS Nano* **2020**, *14*, 13433–13440.
- (17) Sharma, A.; Zhu, Y.; Halbich, R.; Sun, X.; Zhang, L.; Wang, B.; Lu, Y. Engineering the Dynamics and Transport of Excitons, Trions, and Biexcitons in Monolayer WS₂. *ACS Appl. Mater. Interfaces* **2022**, *14*, 41165–41177.
- (18) Datta, K.; Lyu, Z.; Li, Z.; Taniguchi, T.; Watanabe, K.; Deotare, P. B. Spatiotemporally controlled room-temperature exciton transport under dynamic strain. *Nat. Photonics* **2022**, *16*, 242–247.
- (19) Simbulan, K. B.; Feng, Y.-J.; Chang, W.-H.; Lu, C.-I.; Lu, T.-H.; Lan, Y.-W. Twisted Light-Enhanced Photovoltaic Effect. *ACS Nano* **2021**, *15*, 14822–14829.
- (20) Bernardi, M.; Palummo, M.; Grossman, J. C. Extraordinary Sunlight Absorption and One Nanometer Thick Photovoltaics Using Two-Dimensional Monolayer Materials. *Nano Lett.* **2013**, *13*, 3664–3670.
- (21) Gu, J.; Chakraborty, B.; Khatoniari, M.; Menon, V. M. A room-temperature polariton light-emitting diode based on monolayer WS₂. *Nat. Nanotechnol.* **2019**, *14*, 1024–1028.
- (22) Amani, M. et al. Near-unity photoluminescence quantum yield in MoS₂. *Science* **2015**, *350*, 1065–1068.
- (23) Bertolazzi, S.; Brivio, J.; Kis, A. Stretching and Breaking of Ultrathin MoS₂. *ACS Nano* **2011**, *5*, 9703–9709.
- (24) Bukharaev, A. A.; Zvezdin, A. K.; Pyatakov, A. P.; Fetisov, Y. K. Straintronics: a new trend in micro- and nanoelectronics and materials science. *Phys.-Usp.* **2018**, *61*, 1175.
- (25) Michail, A.; Anastopoulos, D.; Delikoukos, N.; Grammatikopoulos, S.; Tsirkas, S. A.; Lathiotakis, N. N.; Frank, O.; Filintoglou, K.; Parthenios, J.; Papagelis, K. Tuning the Photoluminescence and Raman Response of Single-Layer WS₂ Crystals Using Biaxial Strain. *J. Phys. Chem. C* **2023**, *127*, 3506–3515.
- (26) Muoi, D.; Hieu, N. N.; Phung, H. T.; Phuc, H. V.; Amin, B.; Hoi, B. D.; Hieu, N. V.; Nhan, L. C.; Nguyen, C. V.; Le, P. Electronic properties of WS₂ and WSe₂ monolayers with biaxial strain: A first-principles study. *Chem. Phys.* **2019**, *519*, 69–73.
- (27) Yang, J. A.; Bennett, R. K. A.; Hoang, L.; Zhang, Z.; Thompson, K. J.; Michail, A.; Parthenios, J.; Papagelis, K.; Mannix, A. J.; Pop, E. Biaxial Tensile Strain Enhances Electron Mobility of Monolayer Transition Metal Dichalcogenides. *ACS Nano* **2024**, *18*, 18151–18159.
- (28) Conley, H. J.; Wang, B.; Ziegler, J. I.; Haglund, R. F. J.; Pantelides, S. T.; Bolotin, K. I. Bandgap Engineering of Strained Monolayer and Bilayer MoS₂. *Nano Lett.* **2013**, *13*, 3626–3630.
- (29) Schmidt, R.; Niehues, I.; Schneider, R.; Drüppel, M.; Deilmann, T.; Rohlfing, M.; de Vasconcellos, S. M.; Castellanos-Gomez, A.; Bratschitsch, R. Reversible uniaxial strain tuning in atomically thin WSe₂. *2D Mater.* **2016**, *3*, 021011.

- (30) He, X.; Li, H.; Zhu, Z.; Dai, Z.; Yang, Y.; Yang, P.; Zhang, Q.; Li, P.; Schwingschlögl, U.; Zhang, X. Strain engineering in monolayer WS₂, MoS₂, and the WS₂/MoS₂ heterostructure. *Appl. Phys. Lett.* **2016**, *109*, 173105.
- (31) Lee, S. W.; Choi, W. H.; Cho, H.; Lee, S.-h.; Choi, W.; Joo, J.; Lee, D.; Gong, S.-H. Electric-Field-Driven Trion Drift and Funneling in MoSe₂ Monolayer. *Nano Lett.* **2023**, *23*, 4282–4289.
- (32) Stellino, E.; D’Alò, B.; Blundo, E.; Postorino, P.; Polimeni, A. Fine-Tuning of the Excitonic Response in Monolayer WS₂ Domes via Coupled Pressure and Strain Variation. *Nano Lett.* **2024**, *24*, 3945–3951.
- (33) Wang, Y.; Cong, C.; Yang, W.; Shang, J.; Peimyoo, N.; Chen, Y.; Kang, J.; Wang, J.; Huang, W.; Yu, T. Strain-induced direct–indirect bandgap transition and phonon modulation in monolayer WS₂. *Nano Res.* **2015**, *8*, 2562–2572.
- (34) Zhu, C. R.; Wang, G.; Liu, B. L.; Marie, X.; Qiao, X. F.; Zhang, X.; Wu, X. X.; Fan, H.; Tan, P. H.; Amand, T.; Urbaszek, B. Strain tuning of optical emission energy and polarization in monolayer and bilayer MoS₂. *Phys. Rev. B* **2013**, *88*, 121301.
- (35) Mitioglu, A.; Buhot, J.; Ballottin, M. V.; Anghel, S.; Sushkevich, K.; Kulyuk, L.; Christianen, P. C. M. Observation of bright exciton splitting in strained WSe₂ monolayers. *Phys. Rev. B* **2018**, *98*, 235429.
- (36) Mitioglu, A.; Anghel, S.; Ballottin, M. V.; Sushkevich, K.; Kulyuk, L.; Christianen, P. C. M. Anomalous rotation of the linearly polarized emission of bright excitons in strained WSe₂ monolayers under high magnetic fields. *Phys. Rev. B* **2019**, *99*, 155414.
- (37) Thompson, J. J. P.; Brem, S.; Verjans, M.; Schmidt, R.; de Vasconcellos, S. M.; Bratschitsch, R.; Malic, E. Anisotropic exciton diffusion in atomically-thin semiconductors. *2D Mater.* **2022**, *9*, 025008.
- (38) Uddin, S. Z.; Higashitarumizu, N.; Kim, H.; Yi, J.; Zhang, X.; Chrzan, D.; Javey, A. Enhanced Neutral Exciton Diffusion in Monolayer WS₂ by Exciton–Exciton Annihilation. *ACS Nano* **2022**, *16*, 8005–8011.
- (39) Wang, Q.; Maisch, J.; Tang, F.; Zhao, D.; Yang, S.; Joos, R.; Portalupi, S. L.; Michler, P.; Smet, J. H. Highly Polarized Single Photons from Strain-Induced Quasi-1D Localized Excitons in WSe₂. *Nano Lett.* **2021**, *21*, 7175–7182.
- (40) Son, J.; Kim, K.-H.; Ahn, Y. H.; Lee, H.-W.; Lee, J. Strain Engineering of the Berry Curvature Dipole and Valley Magnetization in Monolayer MoS₂. *Phys. Rev. Lett.* **2019**, *123*, 036806.
- (41) Lee, J.; Wang, Z.; Xie, H.; Mak, K. F.; Shan, J. Valley magnetoelectricity in single-layer MoS₂. *Nat. Mater.* **2017**, *16*, 887–891.
- (42) Zhang, Q.; Cheng, Y.; Gan, L.-Y.; Schwingschlögl, U. Giant valley drifts in uniaxially strained monolayer MoS₂. *Phys. Rev. B* **2013**, *88*, 245447.
- (43) Jena, N.; Dimple,; Ahammed, R.; Rawat, A.; Mohanta, M. K.; De Sarkar, A. Valley drift and valley current modulation in strained monolayer MoS₂. *Phys. Rev. B* **2019**, *100*, 165413.
- (44) Jiang, C.; Xiong, W.; Li, C.; Niu, C.; Wang, F. Uniaxial strain induced symmetry lowering and valleys drift in MoS₂. *New J. Phys.* **2021**, *23*, 053007.
- (45) Sodemann, I.; Fu, L. Quantum Nonlinear Hall Effect Induced by Berry Curvature Dipole in Time-Reversal Invariant Materials. *Phys. Rev. Lett.* **2015**, *115*, 216806.
- (46) You, J.-S.; Fang, S.; Xu, S.-Y.; Kaxiras, E.; Low, T. Berry curvature dipole

- current in the transition metal dichalcogenides family. *Phys. Rev. B* **2018**, *98*, 121109.
- (47) Yu, H.; Liu, G.-B.; Gong, P.; Xu, X.; Yao, W. Dirac cones and Dirac saddle points of bright excitons in monolayer transition metal dichalcogenides. *Nat. Commun.* **2014**, *5*, 3876.
- (48) Glazov, M. M. Coherent spin dynamics of excitons in strained monolayer semiconductors. *Phys. Rev. B* **2022**, *106*, 235313.
- (49) Glazov, M. M.; Dirnberger, F.; Menon, V. M.; Taniguchi, T.; Watanabe, K.; Bougeard, D.; Ziegler, J. D.; Chernikov, A. Exciton fine structure splitting and linearly polarized emission in strained transition-metal dichalcogenide monolayers. *Phys. Rev. B* **2022**, *106*, 125303.
- (50) Cooper, R. C.; Lee, C.; Marianetti, C. A.; Wei, X.; Hone, J.; Kysar, J. W. Non-linear elastic behavior of two-dimensional molybdenum disulfide. *Phys. Rev. B* **2013**, *87*, 035423.
- (51) Hybertsen, M. S.; Louie, S. G. Electron correlation in semiconductors and insulators: Band gaps and quasiparticle energies. *Phys. Rev. B* **1986**, *34*, 5390–5413.
- (52) Deslippe, J.; Samsonidze, G.; Strubbe, D. A.; Jain, M.; Cohen, M. L.; Louie, S. G. BerkeleyGW: A massively parallel computer package for the calculation of the quasiparticle and optical properties of materials and nanostructures. *Comput. Phys. Commun.* **2012**, *183*, 1269–1289.
- (53) Enkovaara, J. et al. Electronic structure calculations with GPAW: a real-space implementation of the projector augmented-wave method. *J. Phys.: Condens. Matter* **2010**, *22*, 253202.
- (54) Mortensen, J. J. et al. GPAW: An open Python package for electronic structure calculations. *J. Chem. Phys.* **2024**, *160*, 092503.
- (55) Splendiani, A.; Sun, L.; Zhang, Y.; Li, T.; Kim, J.; Chim, C.-Y.; Galli, G.; Wang, F. Emerging Photoluminescence in Monolayer MoS₂. *Nano Lett.* **2010**, *10*, 1271–1275.
- (56) Qiu, D. Y.; da Jornada, F. H.; Louie, S. G. Optical Spectrum of MoS₂: Many-Body Effects and Diversity of Exciton States. *Phys. Rev. Lett.* **2013**, *111*, 216805.
- (57) Rostami, H.; Roldán, R.; Cappelluti, E.; Asgari, R.; Guinea, F. Theory of strain in single-layer transition metal dichalcogenides. *Phys. Rev. B* **2015**, *92*, 195402.
- (58) Yu, X.-Q.; Zhu, Z.-G.; You, J.-S.; Low, T.; Su, G. Topological nonlinear anomalous Nernst effect in strained transition metal dichalcogenides. *Phys. Rev. B* **2019**, *99*, 201410.
- (59) Sheoran, S.; Jain, M.; Moulik, R.; Bhattacharya, S. Probing the uniaxial strain-dependent valley drift and Berry curvature in monolayer MoSi₂N₄. *Phys. Rev. Mater.* **2023**, *7*, 114003.
- (60) Peng, G.-H.; Lo, P.-Y.; Li, W.-H.; Huang, Y.-C.; Chen, Y.-H.; Lee, C.-H.; Yang, C.-K.; Cheng, S.-J. Distinctive Signatures of the Spin- and Momentum-Forbidden Dark Exciton States in the Photoluminescence of Strained WSe₂ Monolayers under Thermalization. *Nano Lett.* **2019**, *19*, 2299–2312.
- (61) Zhang, X.-X.; Cao, T.; Lu, Z.; Lin, Y.-C.; Zhang, F.; Wang, Y.; Li, Z.; Hone, J. C.; Robinson, J. A.; Smirnov, D.; Louie, S. G.; Heinz, T. F. Magnetic brightening and control of dark excitons in monolayer WSe₂. *Nat. Nanotechnol.* **2017**, *12*, 883–888.
- (62) Robert, C.; Han, B.; Kapuscinski, P.; Delhomme, A.; Faugeras, C.; Amand, T.; Molas, M. R.; Bartos, M.; Watanabe, K.;

- Taniguchi, T.; Urbaszek, B.; Potemski, M.; Marie, X. Measurement of the spin-forbidden dark excitons in MoS2 and MoSe2 monolayers. *Nat. Commun.* **2020**, *11*, 4037.
- (63) Yang, M.; Ren, L.; Robert, C.; Van Tuan, D.; Lombez, L.; Urbaszek, B.; Marie, X.; Dery, H. Relaxation and darkening of excitonic complexes in electrostatically doped monolayer WSe₂: Roles of exciton-electron and trion-electron interactions. *Phys. Rev. B* **2022**, *105*, 085302.
- (64) Wang, G.; Robert, C.; Glazov, M. M.; Cadiz, F.; Courtade, E.; Amand, T.; Lagarde, D.; Taniguchi, T.; Watanabe, K.; Urbaszek, B.; Marie, X. In-Plane Propagation of Light in Transition Metal Dichalcogenide Monolayers: Optical Selection Rules. *Phys. Rev. Lett.* **2017**, *119*, 047401.
- (65) Lin, J.-D.; Lo, P.-Y.; Peng, G.-H.; Li, W.-H.; Huang, S.-Y.; Chen, G.-Y.; Cheng, S.-J. Essential role of momentum-forbidden dark excitons in the energy transfer responses of monolayer transition-metal dichalcogenides. *npj 2D Mater. Appl.* **2023**, *7*, 51.
- (66) Qiu, D. Y.; Cao, T.; Louie, S. G. Non-analyticity, Valley Quantum Phases, and Lightlike Exciton Dispersion in Monolayer Transition Metal Dichalcogenides: Theory and First-Principles Calculations. *Phys. Rev. Lett.* **2015**, *115*, 176801.
- (67) Pedersen, T. G.; Pedersen, K.; Brun Kristensen, T. Optical matrix elements in tight-binding calculations. *Phys. Rev. B* **2001**, *63*, 201101.
- (68) Gomez Sanchez, O. J.; Peng, G.-H.; Li, W.-H.; Shih, C.-H.; Chien, C.-H.; Cheng, S.-J. Enhanced Photo-excitation and Angular-Momentum Imprint of Gray Excitons in WSe₂ Monolayers by Spin-Orbit-Coupled Vector Vortex Beams. *ACS Nano* **2024**, *18*, 11425–11437.
- (69) Barnes, W. L.; Dereux, A.; Ebbesen, T. W. Surface plasmon subwavelength optics. *Nature* **2003**, *424*, 824–830.
- (70) Katzer, M.; Kovalchuk, S.; Greben, K.; Bolotin, K. I.; Selig, M.; Knorr, A. Impact of dark excitons on Förster-type resonant energy transfer between dye molecules and atomically thin semiconductors. *Phys. Rev. B* **2023**, *107*, 035304.
- (71) Robert, C.; Amand, T.; Cadiz, F.; Lagarde, D.; Courtade, E.; Manca, M.; Taniguchi, T.; Watanabe, K.; Urbaszek, B.; Marie, X. Fine structure and lifetime of dark excitons in transition metal dichalcogenide monolayers. *Phys. Rev. B* **2017**, *96*, 155423.
- (72) Oberhauser, D.; Pantke, K.-H.; Hvam, J. M.; Weimann, G.; Klingshirn, C. Exciton scattering in quantum wells at low temperatures. *Phys. Rev. B* **1993**, *47*, 6827–6830.
- (73) Ziegler, J. D.; Zipfel, J.; Meisinger, B.; Menahem, M.; Zhu, X.; Taniguchi, T.; Watanabe, K.; Yaffe, O.; Egger, D. A.; Chernikov, A. Fast and Anomalous Exciton Diffusion in Two-Dimensional Hybrid Perovskites. *Nano Lett.* **2020**, *20*, 6674–6681.
- (74) Zipfel, J.; Kulig, M.; Perea-Causín, R.; Brem, S.; Ziegler, J. D.; Rosati, R.; Taniguchi, T.; Watanabe, K.; Glazov, M. M.; Malic, E.; Chernikov, A. Exciton diffusion in monolayer semiconductors with suppressed disorder. *Phys. Rev. B* **2020**, *101*, 115430.
- (75) Wagner, K.; Zipfel, J.; Rosati, R.; Wittek, E.; Ziegler, J. D.; Brem, S.; Perea-Causín, R.; Taniguchi, T.; Watanabe, K.; Glazov, M. M.; Malic, E.; Chernikov, A. Nonclassical Exciton Diffusion in Monolayer WSe₂. *Phys. Rev. Lett.* **2021**, *127*, 076801.

- (76) Glazov, M. M. Quantum Interference Effect on Exciton Transport in Monolayer Semiconductors. *Phys. Rev. Lett.* **2020**, *124*, 166802.
- (77) Kulig, M.; Zipfel, J.; Nagler, P.; Blanter, S.; Schüller, C.; Korn, T.; Paradiso, N.; Glazov, M. M.; Chernikov, A. Exciton Diffusion and Halo Effects in Monolayer Semiconductors. *Phys. Rev. Lett.* **2018**, *120*, 207401.
- (78) Uddin, S. Z.; Higashitarumizu, N.; Kim, H.; Yi, J.; Zhang, X.; Chrzan, D.; Javey, A. Enhanced Neutral Exciton Diffusion in Monolayer WS₂ by Exciton–Exciton Annihilation. *ACS Nano* **2022**, *16*, 8005–8011.
- (79) Giannozzi, P. et al. QUANTUM ESPRESSO: a modular and open-source software project for quantum simulations of materials. *J. Phys.: Condens.Matter* **2009**, *21*, 395502.
- (80) Perdew, J. P.; Burke, K.; Ernzerhof, M. Generalized Gradient Approximation Made Simple. *Phys. Rev. Lett.* **1996**, *77*, 3865–3868.
- (81) Pizzi, G. et al. Wannier90 as a community code: new features and applications. *J. Phys.: Condens.Matter* **2020**, *32*, 165902.
- (82) Lo, P.-Y.; Peng, G.-H.; Li, W.-H.; Yang, Y.; Cheng, S.-J. Full-zone valley polarization landscape of finite-momentum exciton in transition metal dichalcogenide monolayers. *Phys. Rev. Res.* **2021**, *3*, 043198.